JOURNAL OF THE AMERICAN COLLEGE OF CARDIOLOGY VOL. 74, NO. 9, 2019

^{18}Fluorodeoxyglucose Accumulation in Arterial Tissues Determined by PET Signal Analysis

Rozh H. Al-Mashhadi, MD, PhD,[a,b,c] Lars P. Tolbod, MSc, PhD,[d] Lars Ø. Bloch, MD,[a,e] Martin M. Bjørklund, MD,[a,c,f] Zahra P. Nasr, MSc,[a,c] Zheer Al-Mashhadi, MD,[a] Michael Winterdahl, PhD,[d] Jørgen Frøkiær, MD, DMSci,[a,d] Erling Falk, MD, DMSci,[a,c] Jacob F. Bentzon, MD, PhD[a,c,f]

ABSTRACT

BACKGROUND Arterial ^{18}fluorodeoxyglucose (FDG) positron emission tomography (PET) is considered a measure of atherosclerotic plaque macrophages and is used for quantification of disease activity in clinical trials, but the distribution profile of FDG across macrophages and other arterial cells has not been fully clarified.

OBJECTIVES The purpose of this study was to analyze FDG uptake in different arterial tissues and their contribution to PET signal in normal and atherosclerotic arteries.

METHODS Wild-type and *D374Y-PCSK9* transgenic Yucatan minipigs were fed a high-fat, high-cholesterol diet to induce atherosclerosis and subjected to a clinical FDG-PET and computed tomography scan protocol. Volumes of arterial media, intima/lesion, macrophage-rich, and hypoxic tissues were measured in serial histological sections. Distributions of FDG in macrophages and other arterial tissues were quantified using modeling of the in vivo PET signal. In separate transgenic minipigs, the intra-arterial localization of FDG was determined directly by autoradiography.

RESULTS Arterial FDG-PET signal appearance and intensity were similar to human imaging. The modeling approach showed high accuracy in describing the FDG-PET signal and revealed comparable FDG accumulation in macrophages and other arterial tissues, including medial smooth muscle cells. These findings were verified directly by autoradiography of normal and atherosclerotic arteries.

CONCLUSIONS FDG is taken up comparably in macrophage-rich and -poor arterial tissues in minipigs. This offers a mechanistic explanation to a growing number of observations in clinical imaging studies that have been difficult to reconcile with macrophage-selective FDG uptake. (J Am Coll Cardiol 2019;74:1220–32) © 2019 The Authors. Published by Elsevier on behalf of the American College of Cardiology Foundation. This is an open access article under the CC BY-NC-ND license (http://creativecommons.org/licenses/by-nc-nd/4.0/).

Positron emission tomography (PET) imaging with ^{18}fluorodeoxyglucose (FDG) visualizes glucose uptake in metabolically active tissues. Signal from arteries has been construed as arising predominantly from atherosclerotic plaque macrophages (1,2), and FDG-PET imaging of the ascending aorta and carotid arteries has been used to measure plaque inflammation in randomized clinical trials (3-7). However, the evidence supporting this interpretation of arterial FDG-PET is not complete. Studies of endarterectomy specimens have shown a clear correlation between macrophage content and FDG-PET

Listen to this manuscript's audio summary by Editor-in-Chief Dr. Valentin Fuster on JACC.org.

From the [a]Department of Clinical Medicine, Aarhus University, Aarhus, Denmark; [b]Department of Radiology, Aarhus University Hospital, Aarhus, Denmark; [c]Department of Cardiology, Aarhus University Hospital, Aarhus, Denmark; [d]Department of Nuclear Medicine and PET Center, Aarhus University Hospital, Aarhus, Denmark; [e]MR Center, Aarhus University Hospital, Aarhus, Denmark; and the [f]Centro Nacional de Investigaciones Cardiovasculares Carlos III, Madrid, Spain. This study was supported by the Danish Council for Independent Research/Medical Sciences, Lundbeck Foundation, Danish Heart Foundation, and Aarhus University Research Foundation (AU IDEAS). The CNIC is supported by the Ministerio de Ciencia, Innovación y Universidades, and the Pro CNIC Foundation; and is a Severo Ochoa Center of Excellence (SEV-2015-0505). Dr. Bentzon has served as a consultant for Novo Nordisk A/S; and has within the last 5 years received an investigator-initiated preclinical research grant from Regeneron Pharmaceuticals. All other authors have reported that they have no relationships relevant to the contents of this paper to disclose. Peter Libby, MD, served as Guest Associate Editor for this paper.

Manuscript received December 29, 2018; revised manuscript received June 11, 2019, accepted June 13, 2019.

ISSN 0735-1097 https://doi.org/10.1016/j.jacc.2019.06.057

signal (8-10), but there is no quantitative evidence that macrophages comprise the only or principal site of FDG accumulation in human arteries. On the contrary, studies have revealed nontrivial signal levels arising from arterial segments with few or no macrophages (target to background ratio [TBR] ≈ 1.3 to 1.5) (8-10), and plaque macrophage variation typically accounts for less than one-half of the variation in FDG-PET signal (reported range r^2 = 0.1 to 0.6) (Online Table 1). Other abundant arterial cell types, for example, smooth muscle cells (SMCs), express glucose transporters and take up FDG in vitro (11), but the quantitative contribution of nonmacrophages to the total arterial FDG-PET signal is unknown (1). This complicates the interpretation of clinical FDG-PET trials, because it weakens the underlying tenet that the level and alterations in FDG-PET signal are directly related to inflammation.

SEE PAGE 1233

An important obstacle to understanding the sources of arterial FDG-PET signal is the limited resolution of PET compared with artery wall dimensions (12), which prevents demarcation and direct measurement of signal from arterial subcompartments. Instead, the combined signal from all sources, including background, is typically measured within a region of interest (ROI) around the artery, and this composite measure is correlated empirically with features of interest, for example, plaque macrophages, without further attempts to define the physical origin of the signal.

Detailed investigation of FDG-PET signal sources is difficult to conduct in humans because of the inaccessibility of relevant arteries (e.g., the ascending aorta) to histological analysis. Small animals are also unfavorable, because artery wall dimensions are far below scanner resolution (12). We therefore used *D374Y-PCSK9* transgenic minipigs, which feature arteries and atherosclerotic plaques that are comparable to human arteries and plaques in terms of size and morphology (13-15).

In the present study, we reproduce many findings of human FDG-PET in minipigs, supporting the translational relevance of the animal model. We use a model-based approach for arterial PET signal to estimate the activity fraction of subresolution tissues in vivo (16). Using this approach, we provide estimates of signal arising from separate arterial cellular compartments, and we confirm the accuracy of this approach by tissue autoradiography. Our results show that arterial FDG-PET signal in atherosclerotic minipigs is not dominated by tracer accumulation in macrophages, but rather that FDG accumulates equally in other arterial wall tissues, including SMCs of the arterial media.

METHODS

IN VIVO FDG-PET SCANS. An overview of the animals used in this study is provided in Online Figure 1. Wild-type (WT) (6 male) and transgenic *D374Y-PCSK9* (TG) (5 male, 4 female) minipigs were fed a high-fat, high-cholesterol (HFHC) diet from 8 to 9 weeks of age. Other WT minipigs (4 male) were maintained on a normal diet. At 54 ± 1.8 weeks of age, minipigs underwent FDG-PET and computed tomography (CT) imaging at 186 ± 10 min after injection of 493 ± 28 MBq FDG, followed by euthanasia and histopathological analysis 2 to 4 days later. Pimonidazole (10 mg/kg) was injected in a subgroup of HFHC-fed minipigs (7 TG and 4 WT) at 110 ± 16 min before euthanasia. The atherosclerosis phenotype of the HFHC-fed TG and WT minipigs in the present study has been previously described (13). The Danish Animal Experiments Inspectorate approved all experimental procedures.

AUTORADIOGRAPHY. Four additional TG minipigs (2 male, 2 female) were fed HFHC diet from 8 weeks of age to 80 ± 5 weeks of age and used for autoradiography experiments (Online Figure 1). Pigs were injected with 482 ± 63 MBq FDG and 93 MBq tritium-deoxyglucose, and iliac, carotid, and aortic arteries were extracted after approximately 2 h (Online Figure 2). Three 4-mm blocks from each vessel with visible lesions were chosen for autoradiography. Carotids were lesion-free, and normal blocks were selected. Blocks were snap-frozen, cryosectioned (40 μm), and thaw-mounted onto slides, after which they were dried and apposed onto phosphor imaging plates along with calibrated standards for approximately 5 ^{18}F half-lives. Additionally, 5-μm cryosections were apposed onto imaging plates for a period of 19 weeks to record tritium-deoxyglucose signal. Adjacent sections were processed for immunohistochemistry.

TISSUE ANALYSIS. Aortas were Sudan IV-stained and examined en face to quantify lesion area. Ilio-femoral arteries of in vivo scanned animals were sliced at 1-cm intervals and paraffin-embedded. One longitudinal slice from the major curvature of the ascending aorta was excised and was paraffin embedded. Sections were stained with hematoxylin/eosin or orcein, or with antibodies against muramidase (macrophages) or pimonidazole (hypoxia).

ABBREVIATIONS AND ACRONYMS

CT = computed tomography
FDG = ^{18}fluorodeoxyglucose
HFHC = high-fat, high-cholesterol
PET = positron emission tomography
ROI = region of interest
SMC = smooth muscle cell
SUV = standardized uptake value
TBR = target to background ratio
TG = transgenic
WT = wild-type

In arterial cross sections, the intima and media were manually delineated excluding any calcium deposits, measuring total intima and media areas. Muramidase-positive areas were subtracted to yield macrophage-free intima and media areas. Necrotic areas with low cellularity (<10 cell nuclei per 0.01 mm^2) were also recorded.

IMAGE ANALYSIS. Fused PET/CT images of the ascending aorta, superior vena cava, ilio-femoral arteries, and ilio-femoral veins were analyzed, and careful alignment to tissue specimens was conducted using anatomical landmarks. An ROI was placed around arteries, including lumen, and within the lumen of veins to acquire standardized uptake values (SUV) calculated according to previous reports (17). Standardized total ROI activity (A_{ROI}) inside an ROI was calculated through multiplication of the ROI volume by its average SUV. The background activity, A_{bg} was calculated by multiplying ROI volume by average SUV of the reference vein. Analysis of ilio-femoral arteries were conducted in 12 HFHC-fed minipigs (4 WT and 8 TG), 10 of which had received pimonidazole, while the others were excluded due to spillover signal from the urinary bladder.

STATISTICAL ANALYSIS. Data are represented as mean ± SD. To accommodate any possible grouping effects in regression analyses, the clustered sandwich estimator, with each animal as the grouping variable, was used to estimate robust standard errors (18). A p value cut-off of 0.1 was used for initial selection in stepwise regression with backward elimination. The variance inflation factor was used to assess multicollinearity of independent variables in multivariable regression. Akaike's information criterion was used to evaluate the information loss in regression models. Interobserver agreement for measurements of total vessel wall area (histology), A_{ROI} and A_{bg} (PET images) in ilio-femoral arteries were 4.5 ± 8.2%, 4.7 ± 8.2% and −5.6 ± 5.8% (bias ± SD of bias, Bland-Altman method comparison). Analyses were conducted using Prism version 6 (Graphpad Software Inc., La Jolla, California) and Stata version 15 (StataCorp, College Station, Texas). Significance level was set below 0.05.

Further details on methods are provided in the Online Appendix.

RESULTS

NO DIFFERENCE IN FDG-PET SIGNAL OF HEALTHY AND ATHEROSCLEROTIC ASCENDING AORTAS. The ascending aorta has been used as an important quantification site for plaque inflammation in human FDG-PET trials (3-7), but the dominant source of signal in this arterial segment, which typically has less advanced atherosclerosis (19), is uncertain.

HFHC-fed WT and TG minipigs, like humans, develop mainly early lesion types in the ascending aorta. Age-matched WT minipigs on normal diet were free from atherosclerosis. Using an FDG-PET/CT protocol adapted from clinical studies, we observed strong FDG accumulation in the ascending aorta of all animals with TBRs and SUVs comparable in magnitude to human observations (**Figures 1A to 1F**, Online Figure 3) (17,20). The signal, however, exhibited limited variation with no correlation to the wide range of atherosclerosis present across the 3 groups of minipigs (**Figure 1G**). Importantly, the clear FDG-PET signal from healthy aortas indicated that FDG accumulated in the arterial wall irrespective of the presence of macrophage-containing lesions.

CORRELATIONS BETWEEN PLAQUE MACROPHAGE CONTENT AND FDG-PET SIGNAL REPLICATED IN PIGS. For analysis of arteries with progressive atherosclerotic lesions, we focused on the ilio-femoral arteries. Serial sections from ilio-femoral arteries were stained for macrophages using immunohistochemistry with anti-muramidase antibodies, previously shown to be a reliable macrophage marker in pigs (21), and their locations were carefully aligned to PET/CT slices using anatomic landmarks. Plaque macrophage content correlated significantly with SUV and TBR values, but, as in human studies, the variation in macrophage content could not explain the majority of the variation in arterial PET signal ($r^2 \leq 0.48$) (**Figure 2**). Notably, PET signal was also recorded from vascular segments without macrophages, showing that also in ilio-femoral arteries, signal of nonmacrophage origin played an important role.

SIGNAL MODELING FOR ESTIMATING COMPONENTS OF THE ARTERIAL PET SIGNAL. To identify the unrecognized sites of FDG accumulation, we derived a model for the total arterial PET signal, which is based on the superposition principle and expresses total activity as the sum of all potential signal components. Regression analysis over such a signal model can provide valid estimates of activity fractions originating from sub-resolution tissue components, as recently reported (16).

According to the model, signal must arise from either arterial tissue, residual blood activity, or spillover from neighboring regions:

$$A_{ROI} = C_a \cdot V_a + A_{bg} \quad [1]$$

where A_{ROI} is the standardized (to body weight and tracer dose) total activity in the arterial ROI, V_a is the volume of target arterial tissue, C_a is the recovered

FIGURE 1 **In Vivo FDG-PET of the Ascending Aorta**

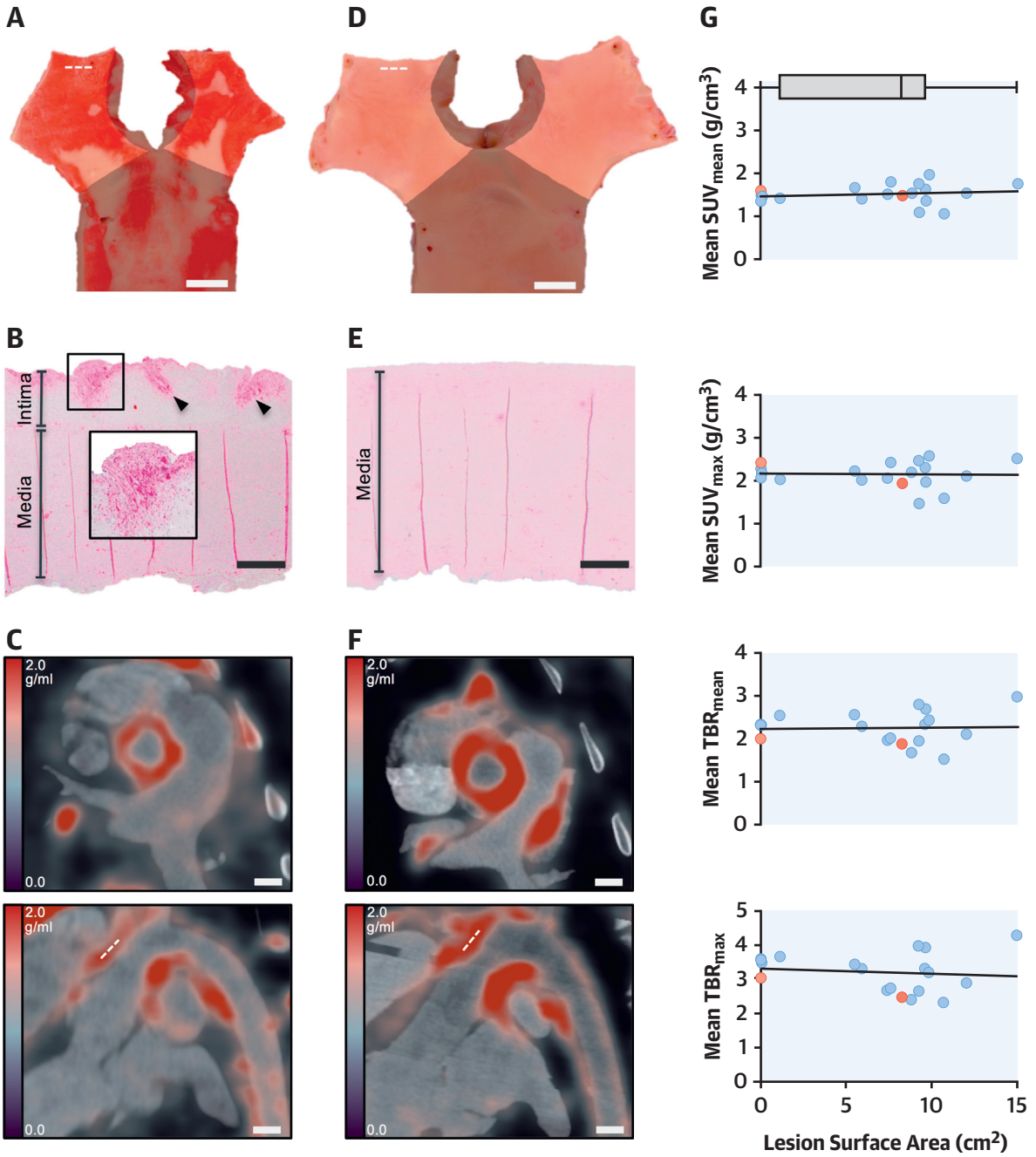

(A) Opened Sudan IV–stained aorta from HFHC-fed transgenic minipig showing atherosclerosis **(red staining)** in the ascending segment **(nonshaded area). (B)** Antimuramidase-stained **(red)** section, obtained at the **dashed lines in A and C,** showing intimal macrophage infiltration **(black arrowheads). (C)** Transsectional **(top)** and longitudinal **(bottom)** reconstructions of fused PET/CT images of the aorta shown in **A. (D)** Lesion-free aorta of a wild-type pig on normal diet. **(E)** Antimuramidase-stained section corresponding to **dashed lines in D and F** showing no macrophages. **(F)** Strong FDG-PET signal from the nonatherosclerotic aorta. Scale bars are 1 cm **(A, C, D, and F)** and 0.5 mm **(B, E)**. PET images are decay corrected and color-coded according to displayed SUV scales **(C, F)**. **(G)** Boxplot showing range of luminal surface lesion area and scatter plots of conventional vascular FDG-PET measures against lesion area (n = 19). Similar PET signal measures are recorded from all arteries, and there are no significant differences between healthy and lesioned aorta groups. The **red and pink markers** reflect arteries shown in **A** and **D**, respectively, displaying similar PET signals. FDG = ^{18}fluorodeoxyglucose; HFHC = high-fat, high-cholesterol; PET = positron emission tomography.

FIGURE 2 **In Vivo FDG-PET of Ilio-Femoral Arteries**

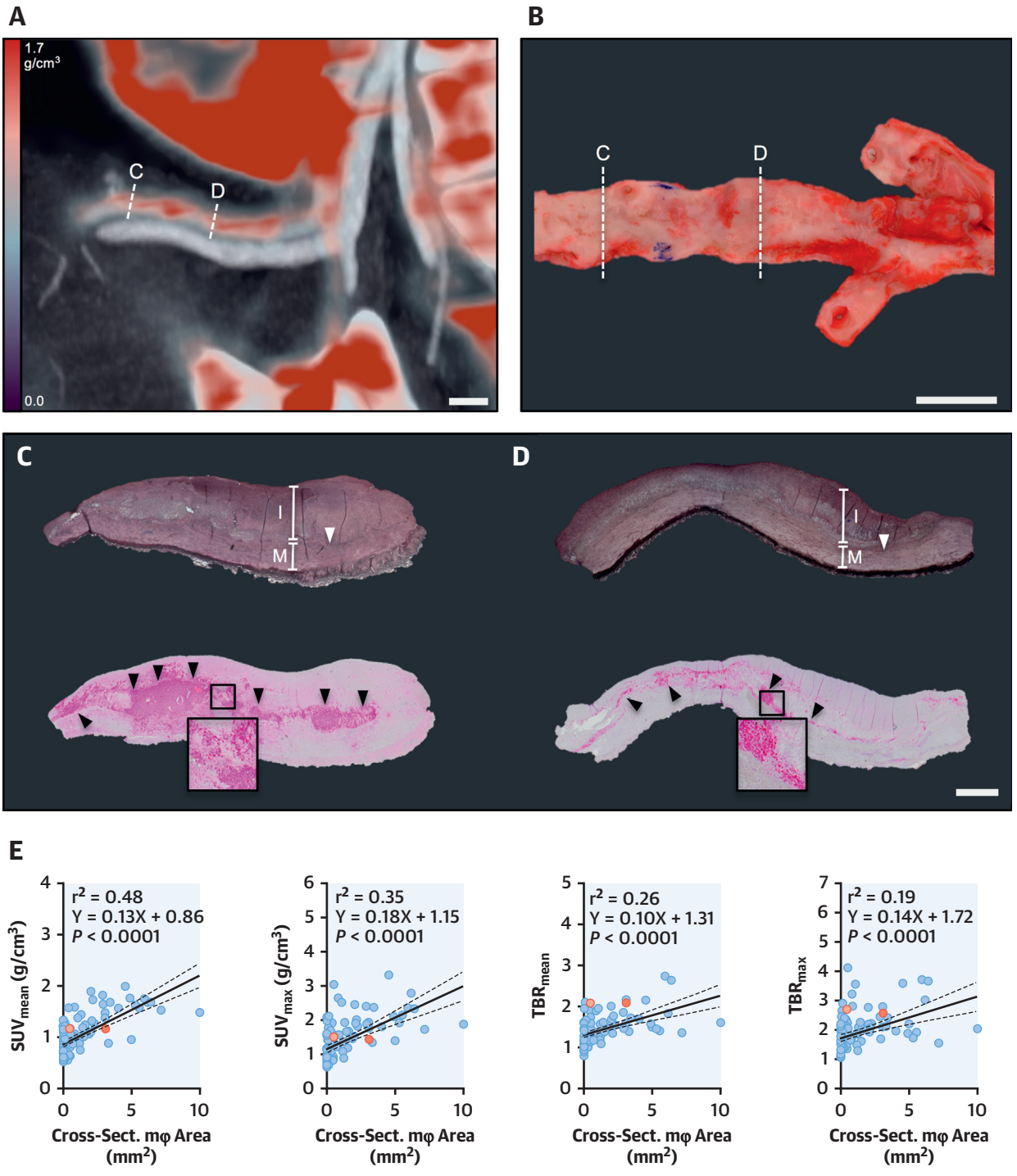

(A) Fused PET/CT image of the right ilio-femoral vessels. **(B)** Opened Sudan IV–stained artery, completely covered by nonraised **(dark red)** or raised **(pink)** lesions. **(C and D)** Cross sections, stained with orcein **(top)** and antimuramidase **(bottom)**, showing large lesions with variable macrophage content **(black arrowheads)**. **White arrowheads** mark the internal elastic membrane. **Dashed lines in A and B** represent locations of **C** and **D**. Scale bars are 1 cm **(A, B)** and 1 mm **(C, D)**. **(E)** Correlations between plaque macrophage area and FDG-PET signal, displayed with 95% confidence bands. The **red and pink markers** reflect tissue slices shown in **C** and **D**, respectively, displaying similar PET signals. Serial sections (n = 115) from 12 minipigs were analyzed. I = intima; M = media; other abbreviations as in Figure 1.

TABLE 1 Model-Based Analysis of FDG-PET Signal

Model	Coefficients	Unit	Robust SE	p Value	95% CI	R^2	AIC
Univariable Models for Individual Arterial Tissue Compartments $A_{ROI} = C_x \cdot V_x + \beta_0$							
1	$C_{m\varphi}$ 11.2	g/cm^3	1.69	0.000	7.44 to 14.9	0.51	−34.7
	β_O 0.69	g	0.04	0.000	0.61 to 0.77		
2	C_{fm} 10.7	g/cm^3	3.40	0.010	3.17 to 18.1	0.16	26.3
	β_O 0.36	g	0.16	0.046	0.01 to 0.71		
3	C_{fi} 5.55	g/cm^3	0.72	0.000	3.96 to 7.15	0.65	−74.9
	β_O 0.64	g	0.03	0.000	0.58 to 0.70		
Multivariable Model Including All Arterial Tissues and Background Signal $A_{ROI} = C_{m\phi} \cdot V_{m\phi} + C_{fm} \cdot V_{fm} + C_{fi} \cdot V_{fi} + A_{bg} + \beta_0$							
4	$C_{m\varphi}$ 2.79	g/cm^3	0.53	0.000	1.63 to 3.95	0.81	−139.1
	C_{fm} 3.08	g/cm^3	1.26	0.033	0.31 to 5.85		
	C_{fi} 2.58	g/cm^3	0.20	0.000	2.13 to 3.03		
	β_O 0.00	g	0.05	0.962	−0.12 to 0.11		

The full signal (Model 4) encompassing all possible signal sources explains much more of the FDG-PET/CT signal than any univariable correlation to individual candidate tissues (Models 1 to 3), as seen by higher determination coefficient (R^2) and lower Akaike's information criterion (AIC). All analyses are based on 115 tissue slices (40 from wild-type and 75 from transgenic pigs fed HFHC-diet). Co-linearity analysis of predictors in model 4 showed variance inflation factors below 2.5.

SE, standard error. A_{ROI} = standardized total activity in the ROI. A_{bg} = standardized total activity of background in the ROI; C = recovered standardized activity concentration of the indicated tissue type; CI = confidence interval; *fm* = macrophage-free media; *fi* = macrophage-free intima; $m\varphi$ = macrophages; β_O = intercept constant; V = tissue volume.

activity concentration in arterial tissue, and A_{bg} is the standardized total activity of the background inside the ROI. The background component represents blood activity and spill-over. It is measured in the reference vein and is assumed to be a good estimate for the arterial background. The arterial tissue can be further split into complementary tissue components, e.g., macrophage-rich tissue ($m\varphi$), macrophage-free media (*fm*), and macrophage-free intima (*fi*):

$$A_{ROI} = C_{m\varphi} \cdot V_{m\varphi} + C_{fm} \cdot V_{fm} + C_{fi} \cdot V_{fi} + A_{bg} \quad [2]$$

Multivariable regression analysis over this signal model was carried out for ilio-femoral arteries with histologically determined subcomponent volumes and measured values of A_{ROI} and A_{bg} (Table 1). This analysis provided a much higher determination coefficient ($R^2 = 0.81$) than any univariable correlation and a nonsignificant intercept that was close to zero, implying that no signal sources were omitted.

As seen from the structure of the signal model equation, and recently validated using simulations and phantom scans (16), the regression coefficients are estimates of the activity concentration that is recovered inside the ROI for macrophage-rich tissue ($C_{m\varphi}$), macrophage-free media (C_{fm}), and macrophage-free intima (C_{fi}). These coefficients were all significantly different from zero, indicating that all tissue types contributed *independently* to the FDG-PET signal. Surprisingly, these estimates were also highly similar, indicating comparable FDG accumulation in different tissue compartments, and opposing the notion of an exceptionally high FDG accumulation in macrophages. The strong correlation between total arterial tissue volume and PET signal is shown graphically in Figure 3A.

ASCENDING AORTA PET SIGNAL DOMINATED BY TRACER ACCUMULATION IN THE ARTERIAL MEDIA. Similar signal modeling was conducted in the ascending aorta comparing lesioned and nonlesioned regions (Online Table 2). We found that the amount of arterial tissue in each region correlated independently with FDG-PET signal, and that the estimated average standardized activity concentrations in both regions were similar. This again indicated that FDG accumulation occurred in bulk arterial tissue, rather than solely in atherosclerotic lesions with macrophage infiltration. This was also consistent with the observed high signal in aortas from healthy minipigs (Figure 1). Due to the thickness of the tunica media (1.74 ± 0.24 mm) compared with the intima (0.20 ± 0.15 mm), the media dominated the total arterial volume, making SMCs of the arterial media the source of the majority of signal even in atherosclerotic aortas. The correlation between total aortic tissue volume and PET signal in the aorta is shown in Figure 3B.

NO CONTRIBUTION TO FDG-PET SIGNAL FROM HYPOCELLULAR REGIONS. FDG accumulates in cells, and hypocellular plaque regions should therefore not contribute noticeably to the PET signal. To test the accuracy of the signal modeling approach, we analyzed the signal contribution of hypocellular regions (fewer than 10 cell nuclei per 0.01 mm^2) (Online Figure 4). The analysis showed no significant

FIGURE 3 Accuracy of Bulk Arterial Tissue as Determinant of FDG-PET Signal in 2 Vascular Beds

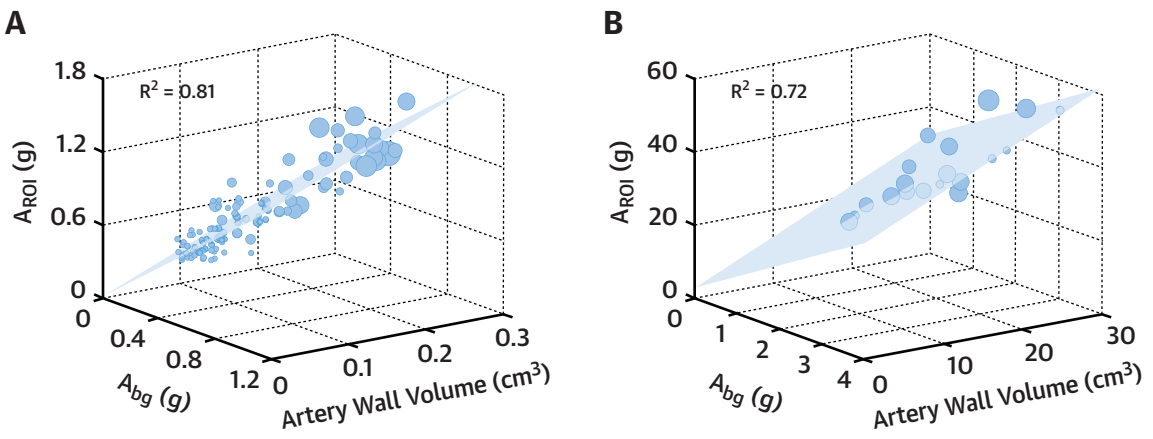

(A) Ilio-femoral arteries from HFHC-fed *D374Y-PCSK9* (n = 8) and wild-type minipigs (n = 4). **(B)** Ascending aortas of HFHC-fed *D374Y-PCSK9* (n = 9) and wild-type minipigs (n = 6), and atherosclerosis-free wildtype minipigs on normal chow (n = 4). Marker diameter is a linear transformation of macrophage volume **(A)** and luminal surface lesion area **(B).** Best fit planes are shown. Abbreviations as in Figure 1.

contribution of hypocellular regions as expected, whereas the rest of the arterial wall retained a highly significant correlation (Online Table 3).

SIGNAL MODEL PREDICTIONS CONFIRMED BY AUTORADIOGRAPHY OF HISTOLOGICAL SECTIONS. Autoradiography is the gold standard to show PET tracer distribution in tissues. To confirm the conclusions of the signal model analysis, we conducted autoradiography of arteries from a new group of atherosclerotic HFHC-fed TG minipigs (n = 4), extracted approximately 2 h after coinjection and in vivo circulation of FDG and tritium-deoxyglucose (Online Figure 2). This allowed the autoradiography to reflect tracer accumulation in tissues at the time point for the FDG-PET scans.

Autoradiographic images showed considerable FDG accumulation in the media of all arteries, including lesion-free carotids, with a signal similar in magnitude to that of the intima/plaque (**Figures 4A to 4D**). Quantification of intima activity concentrations, normalized to the activity concentration of adjacent media, confirmed that intima and media accumulated FDG comparably (**Figure 4E**). To compare FDG uptake in macrophages and macrophage-free intima, we conducted regression analyses across the autoradiographed sections. We found that the volumes of both types of tissues correlated independently with the total intimal activity normalized to macrophage-free media activity concentration. The estimated regression coefficients generally indicated similar activity concentrations in macrophages and macrophage-free media (**Figures 4F to 4H**, Online Table 4).

The autoradiography results thus confirmed the prediction of the signal model that the examined tissues, including normal media, accumulated FDG to a similar extent, and that macrophages did not exhibit exceptional tracer concentrations. Tritium-deoxyglucose autoradiography images agreed with the FDG images, but had lower signal-to-noise levels (Online Figure 5).

MACROPHAGE FDG ACCUMULATION AUGMENTED BY HYPOXIA. Hypoxia has previously been implicated as a modulator of FDG uptake in atherosclerotic plaques (11). Using pimonidazole as a molecular probe, we detected hypoxia mainly in macrophage-rich regions of iliofemoral plaques (Online Figure 6). Because the effect of hypoxia would be to stimulate FDG uptake in cells, we performed exploratory regression analyses using hypoxic volume as interaction terms with macrophage-rich and -free intima. Stepwise regression with backward elimination removed the hypoxia times macrophage-free intima term, but the interaction between macrophages and hypoxia remained in the model with a significant positive coefficient (Online Table 5), indicating that hypoxia may augment FDG accumulation in macrophages.

MACROPHAGE DENSITY NOT INDEPENDENTLY CORRELATED WITH FDG-PET SIGNAL. Macrophage *density* is a variable that has been reported to correlate univariably with FDG-PET signal in human studies (Online Table 1), and we were able to replicate this observation in our data (Online Table 6).

FIGURE 4 Autoradiography

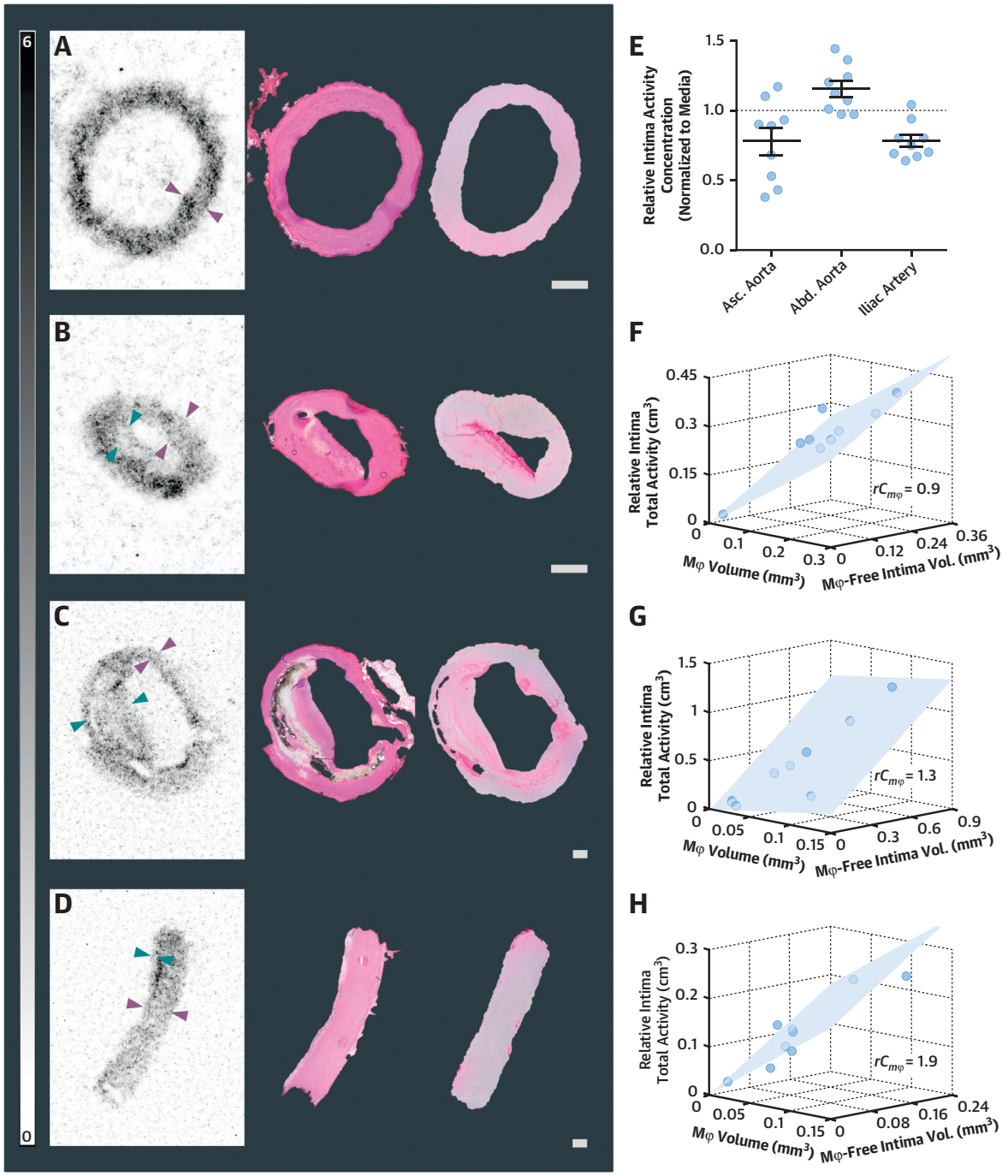

(A to D) FDG autoradiography **(left)** shown with same sections after HE staining **(middle)**, and an adjacent section **(right)** stained for macrophages (muramidase) from the carotid artery **(A)**, iliac artery **(B)**, abdominal aorta **(C),** and ascending aorta **(D)**. Autoradiography images were decay-corrected to injection time and depicted according to the shown scale (Bq/mm^2). **Arrowheads** mark examples of arterial media **(purple)** and intima **(green)**. Scale bars are 1 mm. Note the relatively strong signal from the nonlesioned carotid section **(A)**. **(E)** Relative activity concentration in intima compared with media. Bars are mean ± SEM. **(F to H)** Plots of relative intima activity against volumes of macrophages and macrophage-free intima, showing significant correlations in the iliac arteries **(F)**, abdominal aorta **(G)**, and ascending aorta **(H)** of both tissue types. In each territory, sections with visible intima (n = 9) from 4 HFHC-fed transgenic minipigs were included in the analyses **(E to H)**. $rC_{m\phi}$ = relative macrophage activity concentration normalized to macrophage-free media activity concentration; other abbreviations as in Figure 1.

FIGURE 5 Estimated Contributions of Artery Wall Components to Total FDG-PET Signal

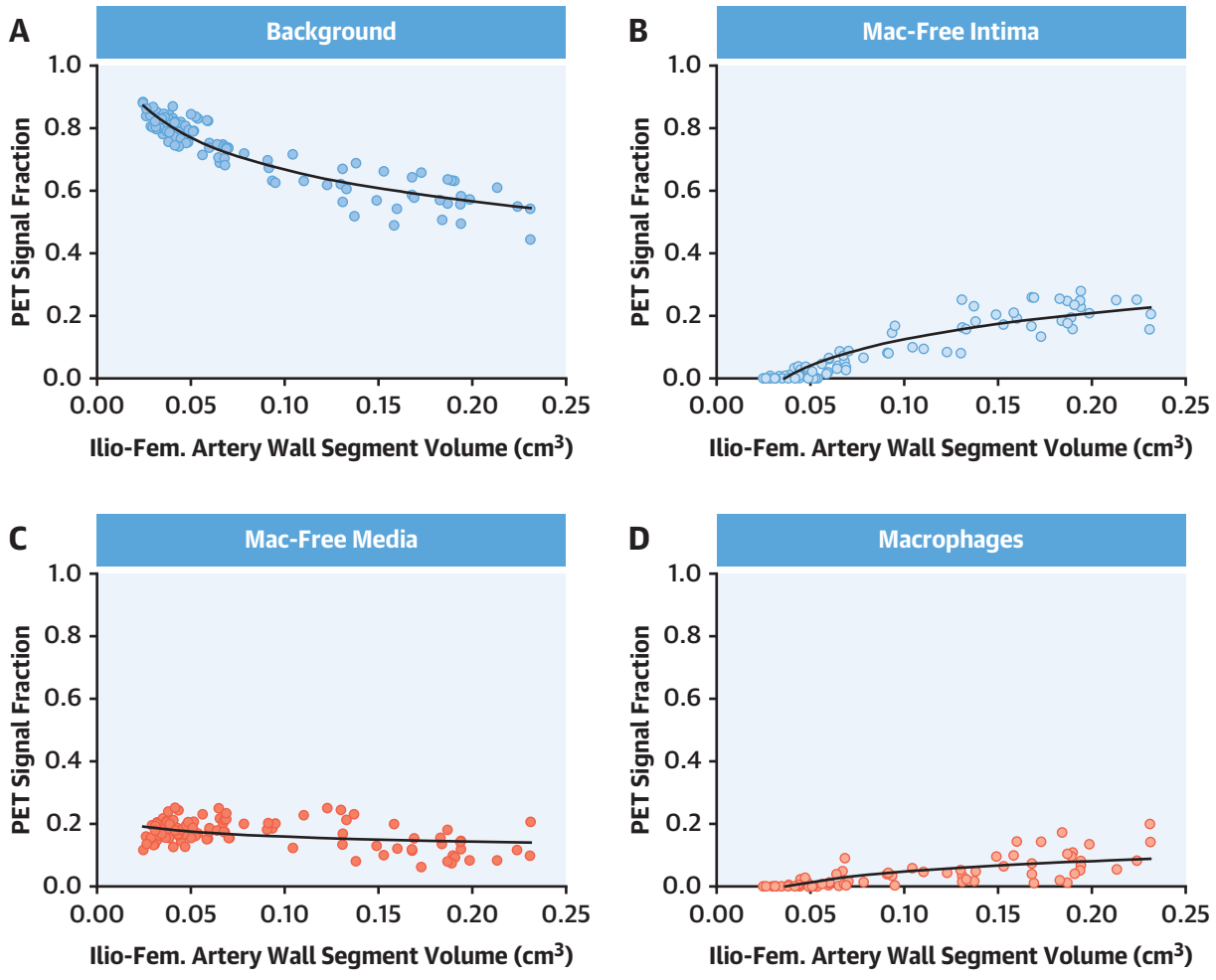

Predicted PET signal fractions originating from different arterial wall components and background in iliofemoral sections (n = 115 sections from 12 pigs). The data are based on the PET signal model 4 regression results presented in Table 1. Fitted semi-log trend lines are presented, $p < 0.0001$ for all lines **(A to D)**. Abbreviations as in Figure 1.

However, this correlation was not independent, but driven by an underlying correlation between macrophage density and total arterial volume ($r^2 = 0.56$). Accordingly, density was rendered insignificant when total volume was included in multivariable analysis (Online Table 6).

ARTERIAL FDG-PET SIGNAL NOT DOMINATED BY MACROPHAGES. The contributions of vessel wall subcomponents to the overall activity in ilio-femoral arteries are shown in Figure 5. The contribution of each arterial component was calculated through multiplication of its volume by its recovered activity concentration, obtained from the signal modeling analysis (Table 1). In atherosclerosis-free arterial segments, the full signal arises from the media and background alone. With the occurrence of lesions, leading to increase in artery wall volume, the artery signal fraction rises while the background fraction recedes. For growing lesions, macrophages gain in relative importance, but the trend lines indicate that macrophages do not become dominant, even for large plaques above 15 mm^2 in cross-sectional area. Online Figure 7 shows the predictions based on the signal model that includes hypoxia in the calculation of the macrophage signal fraction (Online Table 5), but this does not affect the overall pattern.

DISCUSSION

Accurate quantification of disease activity in atherosclerosis is key for identification of individuals at risk and for measuring effects of therapies. Plaque macrophages are relevant to monitor because of their pathophysiological importance in the initiation, progression, and thrombotic complications of atherosclerosis, as well as their responsiveness to antiatherosclerotic therapy (22). Based on the observed correlations between FDG-PET signal and plaque macrophage volume or density (1,2), FDG-PET/CT has been widely used as a noninvasive method to quantify macrophage-driven inflammation in human atherosclerosis (3–7). Previous studies, however, have not been able to quantify all sources of signal from atherosclerotic arteries, and hence cannot rule out that FDG uptake in other cell types could be quantitatively important (1). Indeed, researchers have found that macrophage content explains some of the variation in FDG-PET signal from carotid and femoral arteries with determination coefficients of 0.1 to 0.6 (Online Table 1), but the sources of the residual variation—often the majority—have been unresolved, many probably ascribing a large part of this to noise. The possibility that nonmacrophage tissues may dominate the level and, thus, alterations in arterial FDG-PET signal has not been duly considered in the interpretation of clinical trials.

To address this knowledge gap, we used atherosclerotic minipigs and a signal model for arterial PET, which allowed us to partition the contribution of different types of arterial tissue and background to the composite PET signal. The PET signal model explained the vast majority of signal variation, demonstrating the low level of noise and quantitative power of arterial PET for measuring processes in the arterial wall when conducted in a well-controlled setting and using the quantitative measures of the present study. Importantly, the model-based predictions could be fully confirmed by autoradiography, and the combined body of data showed that FDG accumulation was not predominant in macrophages, but occurred at similar magnitude in other arterial tissues, including healthy arterial media (**Central Illustration**). One important consequence is that in the ascending aorta, where the bulk of tissue is media, only a minority of the FDG-PET signal is derived from cells in atherosclerotic lesions.

CELL TYPES. The arterial tissue partitioning in our analysis was designed to focus on macrophages, but also allows conclusions on SMCs, because the arterial media is a practically pure SMC population. These 2 cell types constitute—by far—the most abundant cell types in the atherosclerotic arterial wall. It would in principle be possible to estimate FDG uptake in other cell types, for example, lymphocytes, by alternative tissue subdivisions, but their lower numbers in typical plaques (23) makes a quantitative important contribution to FDG PET signal less likely.

TRANSLATION FROM MINIPIG EXPERIMENTS TO HUMAN FDG-PET IMAGING. Extrapolating from experimental models to humans is complex, but 2 lines of arguments support the relevance of our findings for human imaging.

First, the conditions and appearance of FDG-PET/CT imaging in minipigs are close to clinical imaging. *D374Y-PCSK9* minipigs develop atherosclerosis with macrophage infiltration, foam cell formation, necrosis, calcification, and fibrous tissue formation (13–15). Also, hypoxia, as shown in the present study (Online Figure 6), has an intraplaque distribution similar to that of human plaques (24). In both pigs and humans, advanced lesions form consistently in the ilio-femoral arteries (13), while the ascending aorta is typically limited to less advanced lesion types (19). Of particular importance for imaging, minipigs resemble humans in terms of body size and vessel dimensions, and thus present similar challenges to imaging with suboptimal resolution (12). We used a scan protocol with late acquisition similar to those used in human studies, and we obtained comparable signal levels with conventional PET quantification measures (17,20). Furthermore, we found univariable correlations between FDG signal and plaque macrophage content consistent with the range of determination coefficients reported in human studies (Online Table 1) (8–10).

Second, the conclusions from our experiments, in particular the significant uptake of FDG in medial SMCs, are consistent with several clinical observations that have hitherto lacked mechanistic explanations. This includes: why PET signal in humans is observed from all vascular sections, including those without macrophages (8–10); why FDG uptake correlates with carotid artery stenosis, irrespective of the degree of inflammation (25); why humans of all ages (5 to 80 years) show FDG accumulation in the aorta (26); and why human aortic signal is relatively high (27), even though atherosclerosis is often limited in this region compared with other vessels (19). It may also help explain why aortic FDG-PET signal is rather stable over time compared with other atherosclerotic arteries (27) and why several clinical trials failed to detect signal changes in the ascending aorta, even when changes in other vessels were present (5,6). Moreover, our findings provide in vivo confirmation

CENTRAL ILLUSTRATION **Cellular Sources of ^{18}Fluorodeoxyglucose-Positron Emission Tomography Signal**

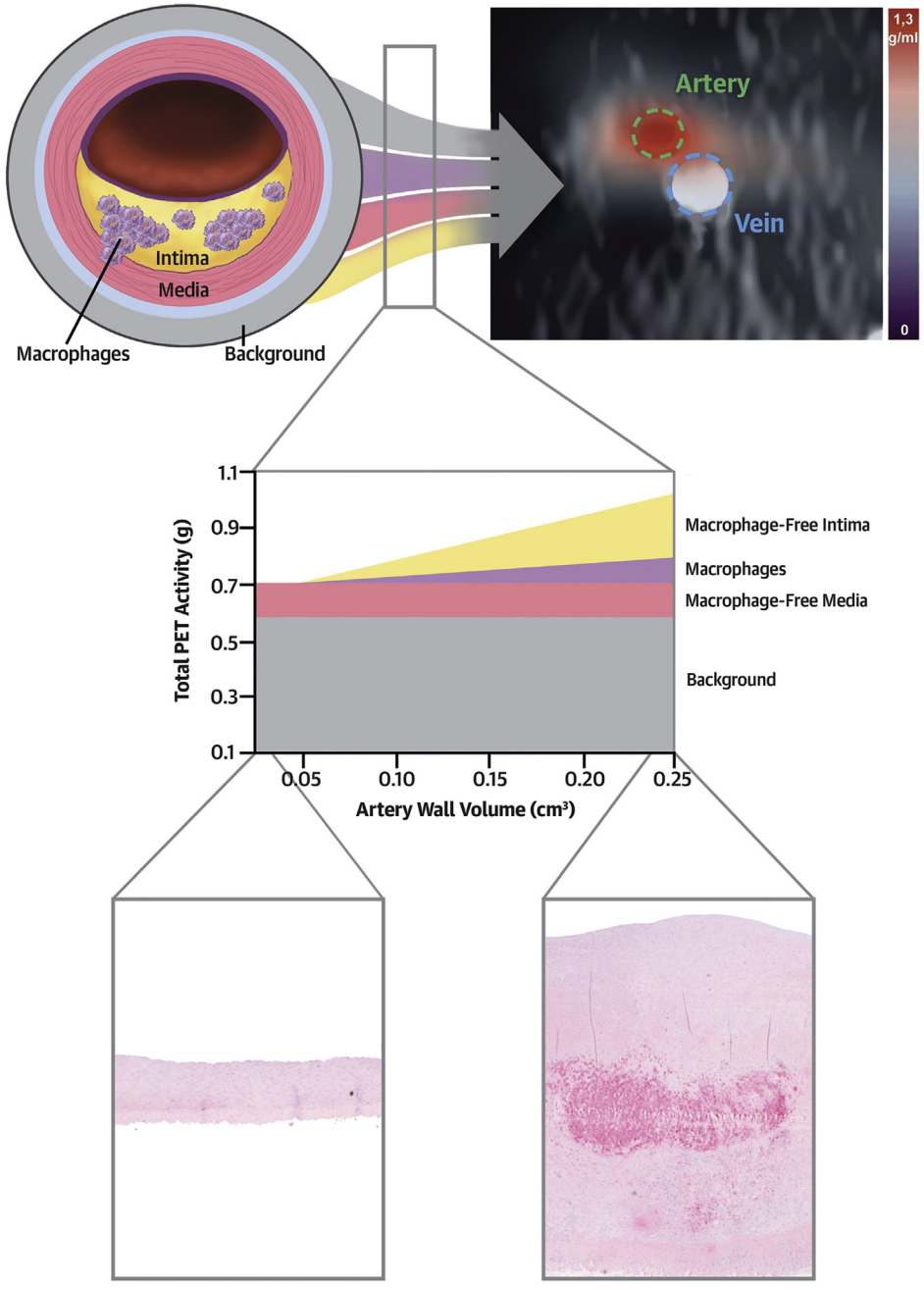

Al-Mashhadi, R.H. et al. J Am Coll Cardiol. 2019;74(9):1220–32.

Top panel: Schematic representation of an arterial cross-section showing an atherosclerotic plaque with macrophage infiltration. Different arterial tissues accumulate similar ^{18}fluorodeoxyglucose (FDG) concentrations leading to comparable positron emission tomography (PET) activity concentrations. **Middle panel:** Schematic representation of total FDG-PET activity as a function of arterial wall volume. Model-based PET analysis allows dissection of the PET signal and identification of the relative contribution of sub-resolution tissues. Macrophages account overall for a minor proportion of the arterial wall total activity. **Bottom panel:** Examples of arterial wall sections with different volumes. **Red stains** show muramidase-positive areas (macrophages).

of hypotheses raised by human cell culture studies, including the comparable glucose uptake of SMCs with macrophages, and the increased glucose uptake in hypoxic macrophages (11).

It is also important to note that our conclusions are not in conflict with any human studies, because there have been no comparable studies of the physical localization of in vivo delivered FDG in human plaques and arterial media at the typical time point for scans. Human carotid endarterectomy specimens have been incubated with radio-labeled deoxyglucose ex vivo (28), but the lack of plaque perfusion/oxygenation and the typical absence of the full arterial media in endarterectomies are important limitations.

IMPLICATIONS FOR CLINICAL FDG-PET TRIALS. Several clinical trials have demonstrated reductions in arterial FDG-PET signal following cholesterol-lowering and other therapies (4,5). Our conclusions are not at odds with these findings, but they suggest that additional mechanisms to alterations in macrophage content or phenotype could be involved. Further studies are needed of how changes in atherosclerotic disease activity are reflected in glucose metabolism of not only macrophages, but also other vascular cells.

Our findings raise particular caution against the use of the ascending aorta as an imaging endpoint, because the thick FDG-accumulating arterial media can overwhelm plaque signal. Recently, an expert group evaluating clinical FDG-PET imaging data also reached the conclusion that the ascending aorta may be less sensitive for detecting effects of interventions (29). We believe that the mechanistic explanation provided in the present study adds further weight to this recommendation.

STUDY LIMITATIONS. Pigs do not develop noteworthy carotid lesions, and we could therefore not investigate the performance of FDG-PET for carotid plaques. Human plaques often have lower total cellularity than the more rapidly evolving plaques in minipigs, and ratios between different cell types may also differ, which could translate into different contributions of the FDG accumulating cell types. However, there is no evidence that human plaques (8–10) are more dominated by macrophages than *D374Y-PCSK9* minipig lesions (**Figure 2**) (14). Furthermore, our data regarding the effect of hypoxia on macrophage FDG accumulation were generated on exploratory basis and need confirmation in future experiments.

CONCLUSIONS

In a large animal model with human-like vessel structure and atherosclerosis, the entire arterial wall, including SMCs in the arterial media, accumulates FDG. This is relevant to consider in the interpretation of FDG-PET/CT trials and may provide mechanistic insight into hitherto poorly understood observations from the clinical imaging literature.

ACKNOWLEDGMENTS The authors thank L.M. Røge and D.W. Qualmann for technical assistance.

ADDRESS FOR CORRESPONDENCE: Dr. Rozh Al-Mashhadi, Department of Radiology, Aarhus University Hospital, Palle Juul-Jensens Boulevard 99, 8200, Aarhus, Denmark. E-mail: rham@clin.au.dk.

PERSPECTIVES

COMPETENCY IN MEDICAL KNOWLEDGE. In a pig model, FDG accumulation is not specific for plaque macrophages, but it occurs in other arterial wall cells as well.

TRANSLATIONAL OUTLOOK: Analysis of PET/CT signals holds promise as a quantitative technique to measure various components of atherosclerotic tissue.

REFERENCES

1. Tarkin JM, Joshi FR, Rudd JHF. PET imaging of inflammation in atherosclerosis. Nat Reviews Cardiol 2014;11:443–57.

2. Dweck MR, Aikawa E, Newby DE, et al. Noninvasive molecular imaging of disease activity in atherosclerosis. Circ Res 2016;119:330–40.

3. Fayad ZA, Mani V, Woodward M, et al. Safety and efficacy of dalcetrapib on atherosclerotic disease using novel non-invasive multimodality imaging (dal-PLAQUE): a randomised clinical trial. Lancet 2011;378:1547–59.

4. Tawakol A, Fayad ZA, Mogg R, et al. Intensification of statin therapy results in a rapid reduction in atherosclerotic inflammation: results of a multicenter fluorodeoxyglucose-positron emission tomography/computed tomography feasibility study. J Am Coll Cardiol 2013;62:909–17.

5. van Wijk DF, Sjouke B, Figueroa A, et al. Nonpharmacological lipoprotein apheresis reduces arterial inflammation in familial hypercholesterolemia. J Am Coll Cardiol 2014;64:1418–26.

6. Emami H, Vucic E, Subramanian S, et al. The effect of BMS-582949, a P38 mitogen-activated protein kinase (P38 MAPK) inhibitor on arterial inflammation: a multicenter FDG-PET trial. Atherosclerosis 2015;240:490–6.

7. Gaztanaga J, Farkouh M, Rudd JHF, et al. A phase 2 randomized, double-blind, placebo-controlled study of the effect of VIA-2291, a 5-lipoxygenase inhibitor, on vascular inflammation in patients after an acute coronary syndrome. Atherosclerosis 2015;240:53–60.

8. Tawakol A, Migrino RQ, Bashian GG, et al. In vivo 18F-fluorodeoxyglucose positron emission tomography imaging provides a noninvasive measure of carotid plaque inflammation in patients. J Am Coll Cardiol 2006;48:1818–24.

9. Figueroa AL, Subramanian SS, Cury RC, et al. Distribution of inflammation within carotid atherosclerotic plaques with high-risk

morphological features a comparison between positron emission tomography activity, plaque morphology, and histopathology. Circ Cardiovasc Imaging 2012;5:69–77.

10. Jezovnik MK, Zidar N, Lezaic L, Gersak B, Poredos P. Identification of inflamed atherosclerotic lesions in vivo using PET-CT. Inflammation 2014;37:426–34.

11. Folco EJ, Sheikine Y, Rocha VZ, et al. Hypoxia but not inflammation augments glucose uptake in human macrophages: Implications for imaging atherosclerosis with ^{18}fluorine-labeled 2-deoxy-D-glucose positron emission tomography. J Am Coll Cardiol 2011;58:603–14.

12. Soret M, Bacharach SL, Buvat I. Partial-volume effect in PET tumor imaging. J Nucl Med 2007;48:932–45.

13. Al-Mashhadi RH, Sørensen CB, Kragh PM, et al. Familial hypercholesterolemia and atherosclerosis in cloned minipigs created by DNA transposition of a human PCSK9 gain-of-function mutant. Sci Transl Med 2013;5:166ra1.

14. Al-Mashhadi RH, Bjørklund MM, Mortensen MB, et al. Diabetes with poor glycaemic control does not promote atherosclerosis in genetically modified hypercholesterolaemic minipigs. Diabetologia 2015;58:1926–36.

15. Shim J, Al-Mashhadi RH, Sørensen CB, Bentzon JF. Large animal models of atherosclerosis-new tools for persistent problems in cardiovascular medicine. J Pathol 2016;238:257–66.

16. Al-Mashhadi RH, Tolbod LP. Quantitative applications in positron emission tomography achieved through signal modelling. Am J Nucl Med Mol Imaging 2019;9:140–55.

17. Bucerius J, Mani V, Moncrieff C, et al. Optimizing 18F-FDG PET/CT imaging of vessel wall inflammation: the impact of 18F-FDG circulation time, injected dose, uptake parameters, and fasting blood glucose levels. Eur J Nucl Med Mol Imaging 2014;41:369–83.

18. Williams RL. A note on robust variance estimation for cluster-correlated data. Biometrics 2000;56:645–6.

19. Agmon Y, Khandheria BK, Meissner I, et al. Independent association of high blood pressure and aortic atherosclerosis: a population-based study. Circulation 2000;102:2087–93.

20. Blomberg BA, Thomassen A, Takx RAP, et al. Delayed ^{18}F-fluorodeoxyglucose PET/CT imaging improves quantitation of atherosclerotic plaque inflammation: results from the CAMONA study. J Nucl Cardiol 2014;21:588–97.

21. Falk E, Fallon JT, Mailhac A, et al. Muramidase: a useful monocyte/macrophage immunocytochemical marker in swine, of special interest in experimental cardiovascular disease. Cardiovasc Pathol 1994;3:183–9.

22. Bentzon JF, Otsuka F, Virmani R, Falk E. Mechanisms of plaque formation and rupture. Circulation Research 2014;114:1852–66.

23. Virmani R, Burke AP, Kolodgie F. Morphological characteristics of coronary atherosclerosis in diabetes mellitus. Can J Cardiol 2006;22 Suppl B:81B–4B.

24. Sluimer JC, Gasc J-M, van Wanroij JL, et al. Hypoxia, hypoxia-inducible transcription factor, and macrophages in human atherosclerotic plaques are correlated with intraplaque angiogenesis. J Am Coll Cardiol 2008;51:1258–65.

25. Shaikh S, Welch A, Ramalingam SL, et al. Comparison of fluorodeoxyglucose uptake in symptomatic carotid artery and stable femoral artery plaques. Br J Surg 2014;101:363–70.

26. Bural GG, Torigian DA, Chamroonrat W, et al. FDG-PET is an effective imaging modality to detect and quantify age-related atherosclerosis in large arteries. Eur J Nucl Med Mol Imaging 2008;35:562–9.

27. Rudd JHF, Myers KS, Bansilal S, et al. (18) Fluorodeoxyglucose positron emission tomography imaging of atherosclerotic plaque inflammation is highly reproducible: implications for atherosclerosis therapy trials. J Am Coll Cardiol 2007;50:892–6.

28. Rudd JHF, Warburton EA, Fryer TD, et al. Imaging atherosclerotic plaque inflammation with [18F]-fluorodeoxyglucose positron emission tomography. Circulation 2002;105:2708–11.

29. van der Valk FM, Verweij SL, Zwinderman KAH, et al. Thresholds for arterial wall inflammation quantified by 18F-FDG PET imaging: implications for vascular interventional studies. J Am Coll Cardiol Img 2016;9:1198–207.

KEY WORDS atherosclerosis, fluorodeoxyglucose, macrophages, PET/CT, signal model

APPENDIX For an expanded Methods section as well as supplemental figures and tables, please see the online version of this paper.